

Compensation of Nonlinear Torsion in Flexible Joint Robots: Comparison of Two Approaches

Michael Ruderman

Abstract—Flexible joint robots, in particularly those which are equipped with harmonic-drive gears, can feature elasticities with hysteresis. Under heavy loads and large joint torques the hysteresis lost motion can lead to significant errors of tracking and positioning of the robotic links. In this paper, two approaches for compensating the nonlinear joint torsion with hysteresis are described and compared with each other. Both methods assume the measured signals available only on the motor side of joint transmissions. The first approach assumes a rigid-link manipulator model and transforms the desired link trajectory into that of the motor drives by using the inverse dynamics and inverse hysteresis map. The second approach relies on the modeling of motor drives and inverse hysteresis and uses the generalized momenta when predicting the joint torsion. Both methods are discussed in details along with a numerical example of two-link planar manipulator under gravity.

I. INTRODUCTION

Joint elasticities in robotic manipulators, see e.g. [1], [2], [3] for details, may provoke the disturbing vibrations of the links but also the relative torsion between the motor drives under control and joint output axes. When the control in joint space operates using the motor drive feedback only, that is the most common case in robotic practice, the relative joint torsion remains uncompensated and leads to the link position errors at heavy loads and large joint torques. The measures of compensating the gravity-induced torsion in robotic joints with linear elasticities have been elaborated and reported in former works [4], [5]. However, when accounting for torsion-torque hysteresis, which is the matter of fact in various geared manipulators and particularly those equipped with harmonic drives, single gravity-related compensation, like one in [6], can be insufficient. This becomes particularly visible when a high positioning accuracy of the links is required. The experimental evidence of torsion-torque hysteresis in a geared single joint with harmonic-drive can be found in e.g. [7], [8]. Further explicit studies of nonlinearities in harmonic-drives can be found in [9], [10], [11], [12], and in the context of robotic joints in the former works [13], [14]. From the last developments in controller design suitable for elastic joint robots, the immersion and invariance (I&I) method [15] can be further mentioned. The method assumes, however, the state feedback available, i.e. position and velocity also of the robot links behind the gear transmission.

This paper makes use of the recently proposed and elaborated joint torsion compensation based on the so-called ‘virtual sensor’ [7], [8], [16], [17]. Two different approaches

are described in the following and compared with each other. The first one is inspired by the feed-forward control law provided in [18]. In the recent paper we extend the reference trajectory transformation and feed-forward control law to the case of nonlinear joint torque with hysteresis. The second approach, based on the previous works [7], [8], [16], observes the actual joint torque from the given motor drive signals and makes a prediction of relative joint torsion by using the inverse hysteresis map. The predicted relative joint torsion, and that with low-pass characteristics, is augmented to the feedback motor drive position, thus providing a ‘virtual’ sensing of link’s position. Both approaches are shown as being integrated into the two-degrees-of-freedom control, including the model-based feed-forwarding and proportion-derivative feedback. We show and compare the control performance of both approaches by using the numerical example of a standard two-link planar manipulator with gravity.

II. DYNAMICS OF ELASTIC JOINT ROBOTS WITH NONLINEARITIES

We consider the flexible joint robotic manipulator as

$$H(q)\ddot{q} + C(q, \dot{q}) + G(q) = \tau(\Delta, t), \quad (1)$$

$$J\ddot{\theta} + \tau(\Delta, t) = u - f(\dot{\theta}), \quad (2)$$

where the left-hand side of the first equation describes the standard rigid-link dynamics, and the second equation describes the joint drives actuated by the vector of motor torques u . The vector of angular coordinates of the link axes is denoted by q , and the vector of angular rotor displacements of the motor drives, reflected through the gear ratios, is denoted by θ . The relative angular displacement between both is denoted by $\Delta = \theta - q$ and constitutes the vector of joint torsion. The schematic representation of an elastic robotic joint described by (1), (2) is illustrated in Fig. 1. Note

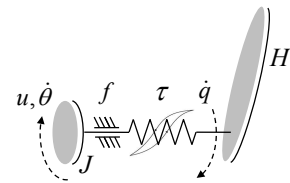


Fig. 1. Elastic robotic joint with hysteresis and friction nonlinearities

that if assuming the linear joint stiffness, i.e. $\tau = K\Delta$ where K is a positive diagonal matrix, and neglecting the nonlinear motor drive friction f , the model (1), (2) reduces to the well-established model of elastic joint robots initially proposed by

M. Ruderman is with Department of Electrical, Electronics, and Information Engineering, Nagaoka University of Technology, 1603-1, Kamitomioka, Nagaoka, 940-2188 Japan ruderman@vos.nagaokaut.ac.jp

Spong in [5]. The rigid-link dynamics is parameterized by $H(q) \in \mathbb{R}^{n \times n}$ inertia matrix of manipulator and $C(q, \dot{q}) \in \mathbb{R}^n$ and $G(q) \in \mathbb{R}^n$ vectors of Coriolis/centrifugal and gravity torques correspondingly. $J = \text{diag}(j_i) \in \mathbb{R}^{n \times n}$ is the positive diagonal matrix of motor drive inertias. The objective of our model extension is to capture the nonlinear joint elasticities with hysteresis, as will be shown further in Section III. Heretofore we will keep, however, the joint torque τ as a generic nonlinear function of relative torsion and time, hence without loss of generality.

To keep the modeling of motor drives friction simple as possible while capturing, at the same time, the most pronounced friction nonlinearities we apply the steady-state Stribeck friction curve. Note that a more complex (dynamic) friction behavior includes the phenomenon of friction lag, also known as hysteresis in the velocity, and the presliding hysteresis in displacement, see e.g. [19], [20] for details. The total friction torque of the i -th motor drive¹ is described by

$$f(\dot{\theta}) = \text{sig}(\dot{\theta}) \left(F_c + F_s \exp[-V^{-\mu} |\dot{\theta}|^\mu] \right) + B\dot{\theta}. \quad (3)$$

Here the standard Stribeck characteristic curve is parameterized by the Coulomb and Stribeck friction coefficients $F_c > 0$ and $F_s > 0$ correspondingly. The exponential parameters $\mu \neq 0$ and $V > 0$ are respectively the Stribeck velocity and shape factors; both determine the velocity weakening and strengthening curve. The linear viscous friction coefficient is denoted by B . Note that the applied sigmoid function

$$\text{sig}(\dot{\theta}) = \frac{2}{1 + \exp(-\gamma\dot{\theta})} - 1 \quad (4)$$

allows avoiding the discontinuity at zero velocity crossing, while γ is the velocity scaling factor.

III. REFERENCE TRAJECTORY TRANSFORMATION

The first approach relies on the model-based transformation between the given link reference q_r and motor-drive reference θ_r , which is provided to the feedback control. Furthermore, the feed-forward control in the transformed θ_r coordinates is used. As has been shown in [18], the reference trajectory of the desired robot link position can be transformed into that of the motor drives by using the inverse model of rigid-link dynamics and inverse matrix of joint stiffness coefficients. Since the joint elasticities are not longer linear we are to extend the reference trajectory transformation to the general case of a nonlinear torsion-torque map $\tau = \chi(\Delta)$. Given the reference link trajectory $q_r(t) \in \mathcal{C}^4$ one obtains the desired motor drive trajectory as

$$\theta_r = q_r + \chi^{-1}(\tau_r), \quad (5)$$

where the reference joint torque τ_r is computed according to (1). Differentiating twice with respect to the time, whilst

¹Note that here and further in (4) we skip the index i for the sake of simplicity, while a scalar value, computation is meant.

taking into account the rate-independency of hysteresis, i.e. $\frac{d}{dt} \partial \chi^{-1} / \partial \tau = 0$, one obtains

$$\ddot{\theta}_r = \ddot{q}_r + \frac{\partial \chi^{-1}}{\partial \tau_r} \ddot{\tau}_r. \quad (6)$$

One can see that in order to realize the motor drive reference (6) the corresponding joint link reference should be at least 4 times differentiable since

$$\ddot{\tau}_r = H(q_r) q_r^{(4)} + 2\dot{H}(q_r) q_r^{(3)} + \ddot{H}(q_r) \ddot{q}_r + \ddot{C}(q_r, \dot{q}_r) + \ddot{G}(q_r). \quad (7)$$

Now, having the reference trajectory transformation, and with respect to the motor drive dynamics (2), one obtains the reference feed-forward control as

$$u_r = J\ddot{\theta}_r + \chi(\theta_r - q_r) + f(\dot{q}_r) \equiv J\ddot{\theta}_r + \tau_r + f(\dot{q}_r). \quad (8)$$

Note that the friction compensating term is included in (8) while assuming $f(\dot{q}) \approx f(\dot{\theta})$ for the reference value. This is justified at least for non-zero velocities, i.e. apart from the motion reversals.

IV. OBSERVATION OF JOINT TORSION

The second approach relies on the fact that the reactive joint torque appears as an input disturbance of the motor drives under control. Assuming the model of motor drives is given and the input-output data tuples $(u + \tau, \dot{q})$ are available from the measurement, the input disturbance τ can be detected and isolated by using the method of so-called generalized momenta, see [21], [22] for details.

Introducing the vector of generalized momenta $p = J\dot{\theta}$ we rewrite the motor drive dynamics (2) as

$$\dot{p} = u - f(\dot{\theta}) - \tau. \quad (9)$$

Since the drive and friction torques are known from the measurement, the dynamics of generalized momenta can be estimated by

$$\dot{\hat{p}} = u - f(\dot{\theta}) - r, \quad (10)$$

where the residual vector $r = L(\hat{p} - p)$ is proportional to the estimation error. The diagonal matrix $L > 0$ is a design parameter. Note that (10) is a standard observer for the class of dynamic systems with nonlinear term, here friction, as a function of measurable outputs [22]. Further it can be shown that since

$$r = L \left(\int [u - f(\dot{\theta}) - r] dt - p \right), \quad (11)$$

the residual state dynamics complies with

$$\dot{r} + Lr = L\tau. \quad (12)$$

It is evident that the residual state r follows the unknown joint torque and, by doing this, exhibits the first-order time delay behavior with the time constants L^{-1} .

The detected and isolated reactive joint torque $\tilde{\tau} = r$ serves as the input of inverse hysteresis model

$$\tilde{\Delta}(\tilde{\tau}) = \alpha^{-1} \left(W^{-1} [\tilde{\tau} - (I - W)\beta(\tilde{\Delta})] \right), \quad (13)$$

where α and β are the static and dynamic terms of the Bouc-Wen-like hysteresis model, see [23], [7] for details. $W = \text{diag}(w_i) \in \mathbb{R}^{n \times n}$ is the diagonal matrix of weighting factors $0 < w_i < 1$ and I is the identity matrix. The static term of Bouc-Wen-like hysteresis model is given by

$$\bar{\tau}_i = \alpha(\Delta_i) = k_1 \Delta_i + k_3 \Delta_i^3, \quad (14)$$

and captures the stiffening spring characteristics. The dynamic term

$$\hat{\tau}_i = \beta(\Delta_i) = k_1 \int \dot{x}_i dt + k_3 \left(\int \dot{x}_i dt \right)^3 \quad (15)$$

with an internal state

$$\dot{x}_i = \dot{\Delta}_i - \psi |\dot{\Delta}_i| |x_i|^{\eta-1} x_i - \xi \dot{\Delta}_i |x_i|^\eta \quad (16)$$

captures the actual hysteresis state and is parameterized by the hysteresis control parameters ψ , ξ , and η . The parameters k_1 and k_3 are the linear and cubic stiffness coefficients. Note that the relationship between a purely elastic and purely plastic (hysteresis) contributions is determined by the weighting factor w . Assuming the Bouc-Wen-like torsion-torque hysteresis is given (identified) and reactive joint torque is observed, the vector of joint torsion can be computed online by (13). For more details on this method, also denoted as virtual sensor of joint torsion, and its experimental evaluation the reader is referred to [7], [8].

An independent joint control with the motor drive feedback and virtual sensor of joint torsion is given by

$$u = K_p e + K_d \dot{e} + K_p \tilde{\Delta}(\tilde{\tau}), \quad (17)$$

where K_p and K_d are the positive diagonal matrices of proportion and derivative control gains, and $e = q_r - \theta$ is the control error in the joint link space. It is easy to recognize that the proportional control part operates on the $q_r - \theta + \tilde{\Delta}$ error quantity, and once $\tilde{\Delta} = \Delta$ correspondingly on $q_r - q$. Therefore the steady-state error of feedback control (17), in the joint link space, will be the same as the residual error of predicting the relative joint torsion. Important to note is that since the $\tilde{\tau}/\tau$ transfer characteristics constitutes a low-pass filter, the feedback of $\tilde{\tau}$, mapped through the hysteresis function, cannot destabilize the closed-loop system. Recall that the hysteresis map $\tilde{\tau} \mapsto \tilde{\Delta}$ by itself serves as an additional rate-independent damping, see e.g. [24]. In the rest of this Section, we will prove the stability assumption made above for the weaker condition $\tilde{\Delta} = K^{-1} \tilde{\tau}$, i.e. without additional hysteresis damping. In the following we assume that the joint couplings and configuration-dependent nonlinearities of manipulator dynamics are compensated by the model-based feed-forwarding. Furthermore, we approximate the motor drive friction by the linear viscous friction $f \approx B \dot{\theta}$ which is appropriate except for the motion reversals.

The linearized model of the i -th elastic robotic joint² can be written in Laplace s -domain as

$$P_l(s)q(s) = K\theta(s), \quad (18)$$

$$P_m(s)\theta(s) = u(s) + Kq(s), \quad (19)$$

²Note that here and for the rest of this Section we skip the index i for the sake of simplicity, while scalar value computations are meant.

where

$$P_l(s) = \hat{H}s^2 + K, \quad (20)$$

$$P_m(s) = Js^2 + Bs + K \quad (21)$$

are the forward transfer functions of the joint links and motor drives correspondingly. The forward and feedback couplings between both are provided by the joint stiffness K . The linearized (decoupled) inertia of manipulator links is denoted by \hat{H} . When using the predicted joint torsion in feedback, i.e. $u = K_p \tilde{\Delta}$, the motor drive equation (19) becomes

$$\left(P_m - \frac{K_p}{L^{-1}s + 1} \right) \theta(s) = u(s) + \left(K - \frac{K_p}{L^{-1}s + 1} \right) q(s). \quad (22)$$

Considering the open-loop system (18), (22) one can rewrite the characteristic polynomial of the transfer function $\theta(s)/u(s)$ into the form

$$1 + K_p G(s) = 0, \quad (23)$$

where

$$G(s) = \frac{K - (\hat{H}s^2 + K)((L^{-1}s + 1)(Js^2 + Bs + K) - 1)}{K^2(L^{-1}s + 1)}. \quad (24)$$

The root locus of characteristic polynomial (24) is exemplarily shown in Fig. 2 together with the pole-zero diagram of the nominal plant (18), (19). One can see that when increasing the feedback gain K_p the critical, i.e. from stability point of view, pole moves towards the conjugate-complex zeros of nominal plant. Here, a relatively large gain variation is possible without entering the marginally-stable region close to imaginary axis. One should note that the variation of L , which is equally a design parameter, reshapes the root locus trajectories so that an admissible K_p range will equally change. However, it is obvious that the feedback of predicted joint torsion is not destabilizing the transfer characteristics of elastic robotic joint. A suitable trade-off between L and K_p can be found during the first stage of the control design, i.e. before closing the feedback loop by the PD term.

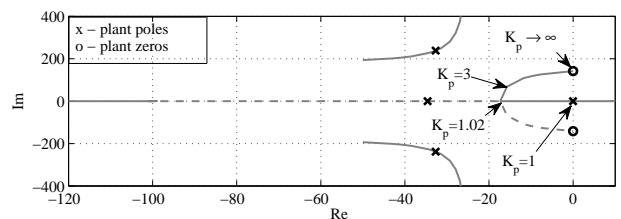


Fig. 2. Root locus (with respect to K_p) of elastic joint extended by VS, i.e. (18), (22), versus pole-zero diagram of the nominal plant (18), (19)

V. NUMERICAL EXAMPLE

Consider a classical example of two-link planar manipulator with revolute joints under impact of gravity as shown in Fig. 3. Note that this structure is particularly interesting since coinciding with the ‘shoulder’ and ‘elbow’ axes of several anthropomorphic, also known as RRR, industrial robotic manipulators. The detailed deviation of kinematics

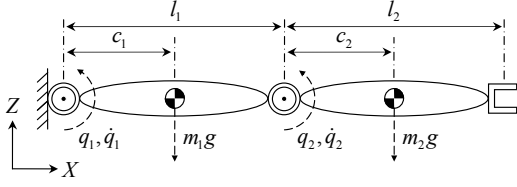


Fig. 3. Two-link planar manipulator under gravity

and dynamics of a two-link planar manipulator under gravity can be found in e.g. [2], [3]. Here we note that c_1 and c_2 are the distances of the center of mass of both links to the corresponding joint axes. The length of the links are denoted by l_1 correspondingly l_2 . The moments of inertia of the links, relative to their center of mass, are denoted by I_1 and I_2 respectively. Further, for the sake of simplicity, we assume $l_1 = l_2 = l$, $c_1 = c_2 = 0.5l$, $I_1 = I_2 = I$, and $m_1 = 2m_2 = m$. For the dynamics of rigid two-link planar manipulator, described explicitly e.g. in [2], [3], and assumptions made above we obtain the elements of H matrix and C and G vectors as following:

$$\begin{aligned}
 h_{11} &= ml^2(0.875 + 0.5 \cos q_2) + 2I, \\
 h_{12} = h_{21} &= ml^2(0.25 + 0.5 \cos q_2) + I, \\
 h_{22} &= 0.25ml^2 + I, \\
 c_1 &= -0.5ml^2 \sin q_2 (2\dot{q}_2 \dot{q}_1 + \dot{q}_2^2), \\
 c_2 &= 0.5ml^2 \sin q_2 \dot{q}_1^2, \\
 g_1 &= mlg(1.5 \cos q_1 + 0.5 \cos(q_1 + q_2)), \\
 g_2 &= 0.5mlg \cos(q_1 + q_2). \quad (25)
 \end{aligned}$$

The parameters assumed for numerical simulation are listed in Table I. Note that several nonlinear parameters, like the shape factors of Stribeck curve and hysteresis, are assumed to have the same values for both axes, this for the sake of simplicity. Further we note that, for the sake of comprehensibility, the parameters related to the joint transmission are denoted with ‘deg’ and not ‘rad’ units as otherwise. The corresponding f - θ friction and τ - Δ hysteresis curves are visualized in Fig. 4 (a) and (b) correspondingly.

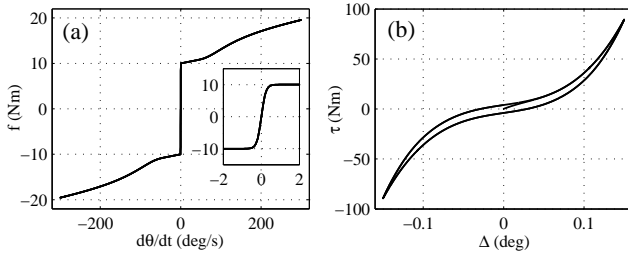


Fig. 4. Characteristic curves of nonlinear friction (a) and hysteresis (b)

The following results are obtained within numerical simulation of the robot plant according to (1), (2), (25) plus an additional viscous joint damping D so that $\tau = \chi(\Delta) + D\dot{\Delta}$. Note that the latter is also required for stabilizing the numerically implemented hysteresis (13)-(16) at steeply

TABLE I
PLANT PARAMETERS USED IN NUMERICAL SIMULATION

Parameter	Unit	Value
J	kg m ²	$[1, 1]^T$
I	kg m ²	0.5
g	m s ⁻²	9.8
m	kg	10
l	m	0.5
F_c	Nm	$[10, 10]^T$
F_s	Nm	$[5, 5]^T$
B	Nm s rad ⁻¹	$[1, 1]^T$
V	s rad ⁻¹	$[2, 2]^T$
μ	unitless	$[-2, -2]^T$
γ	unitless	$[500, 500]^T$
D	Nm s deg ⁻¹	$[1, 1]^T$
K_1	Nm deg ⁻¹	$[300, 300]^T$
K_3	Nm deg ⁻¹	$[50000, 50000]^T$
w_i	unitless	$[0.4, 0.4]^T$
ψ	unitless	$[300, 300]^T$
ξ	unitless	$[500, 500]^T$
η	unitless	$[1.5, 1.5]^T$

changes of the torsion value, e.g. at higher steps of the applied input torque. Furthermore, in order to render more realistic conditions of the motor drive feedback control, the manipulator plant signals θ_1 and θ_2 are outputted through the 14 bit per revolution quantization blocks, that is adequate for the common motor drive encoders.

The effect of complex nonlinear dynamics of two-link planar manipulator is visualized by means of a ‘free fall’ response. This one assumes the initial joint configuration $\theta(t_0) = [0, 0]$ deg which is the horizontal (outstretched) manipulator pose with the maximal gravity acting on both axes. The free fall response is shown in Fig. 5, for the 1st joint on the left and 2nd joint on the right. The position trajectories are shown in Fig. 5 (a) and (e). Note that the second joint stops its large displacement earlier than the first one, mainly due to the friction. The micro-displacements, visible in torsion response in Fig. 5 (b) and (f) exhibit however nearly the same duration for both joints. Remarkable is the fact of hysteresis lost motion (non-zero torsion) at steady-state. The phase portrait in the $(\theta, \dot{\theta})$ coordinates are shown in Fig. 5 (c) and (g). The zoom-in of both trajectories in vicinity to final equilibrium are depicted in Fig. 5 (d) and (h). One can see that after the motion response on a ‘fast’ time scale, including both the transients and ‘quasi steady-states’ up to about $t = 5$ s, an extremely slow relaxation of nonlinear (creeping) dynamics occurs. The final equilibrium is achieved after about $t = 900$ s while the overall creeping displacement is about 1 deg for the 1st joint and 9 deg for the 2nd one. The observed creeping phenomenon occurs mainly due to an interplay between the hysteresis restoring torque and friction torque nonlinearities. Here we note that no stiction force is captured by (3) and (4) and, in reality,

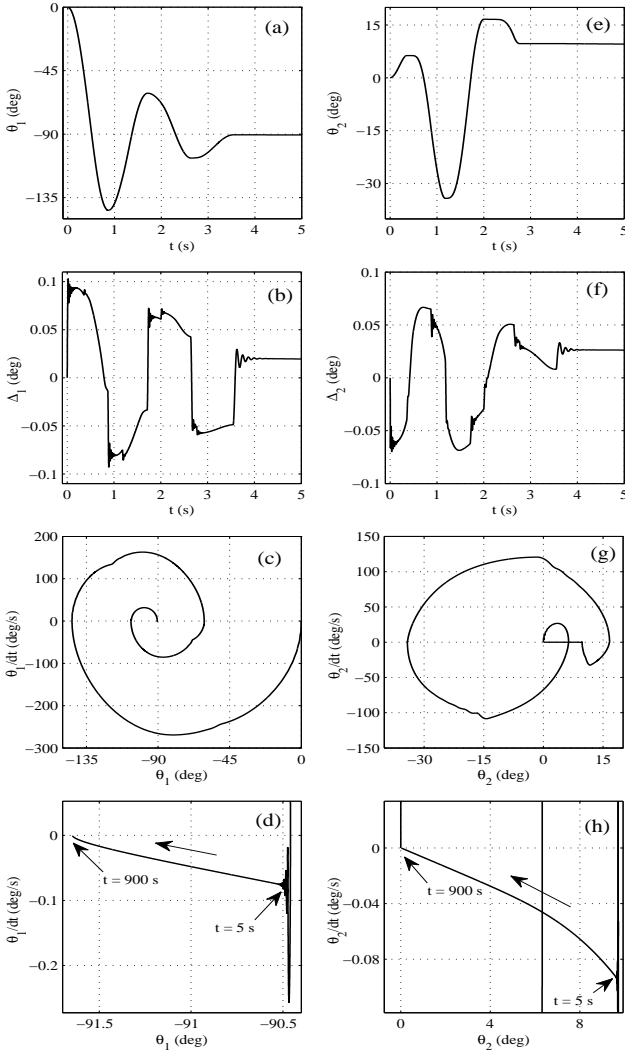


Fig. 5. Free fall response of two-link manipulator joints from $\theta(t_0) = [0, 0]$ deg: 1st joint on the left and 2nd joint on the right. (a), (e) motor drive position θ ; (b), (f) joint torsion Δ ; (c), (g) state trajectories $(\theta, \dot{\theta})$; (d), (h) zoom-in of $(\theta, \dot{\theta})$ trajectories at slow relaxation dynamics.

the joints may stop without exhibiting a slow relaxation dynamics.

In the first approach (further denoted as ‘Control I’), the full-order feed-forward control (8) is combined with the standard PD feedback control so that the overall control law becomes

$$u = K_p(\theta_r - \theta) + K_d(\dot{\theta}_r - \dot{\theta}) + u_r(\theta_r), \quad (26)$$

where the reference θ_r is obtained from q_r through the trajectory transformation as described in Section III.

In the second approach (further denoted as ‘Control II’), the control law (17) is combined with the reduced-order feed-forwarding as that

$$u = K_p e + K_d \dot{e} + K_p \tilde{\Delta}(\tilde{\tau}) + \tilde{u}_r, \quad \text{with} \quad (27)$$

$$\tilde{u}_r = (H(q_r) + J)\ddot{q}_r + C(q_r, \dot{q}_r) + G(q_r) + f(\dot{q}_r).$$

Note that the feed-forward control part \tilde{u}_r is not explicitly accounting for joint elasticities. The setup control gains used

for both, Control I and Control II, plus the observer gain are listed in Table II.

TABLE II
CONTROL PARAMETERS USED IN NUMERICAL SIMULATION

K_p (Nm rad ⁻¹)	K_d (Nm rad ⁻¹ s)	L
$[1.3, 1.3]^T$	$[0.43, 0.43]^T$	$[100, 100]^T$

The evaluated trajectory constitutes a simultaneous motion of both links with the same shape of joint references $q_{(1,2),r} \in \mathcal{C}^4$ as depicted in Fig. 6 (a). In order to visualize the

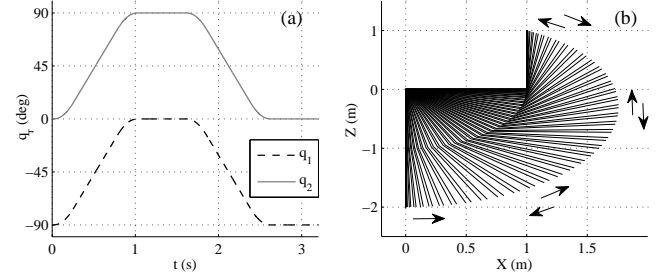


Fig. 6. Evaluated trajectory in the joint space (a) and Cartesian space (b)

motion of two-link manipulator in the operational (Cartesian) space, and thus convey an impression about the corresponding joint loads, we make use of the forward kinematics of two-link planar manipulator according to [2]. This is quite trivial and can be derived by using a geometric approach as follows. Given the joint coordinates q_1 and q_2 the Cartesian coordinates are given by

$$X = l \cos q_1 + l \cos(q_1 + q_2), \quad (28)$$

$$Z = l \sin q_1 + l \sin(q_1 + q_2). \quad (29)$$

The stroboscopic motion of two-link planar manipulator with the start configuration $q_r(t_0) = [-90, 0]$ deg and end configuration $q_r(t_{3.2}) = [-90, 0]$ deg, coming through the upper steady-state position $q_r(t_{1.1-1.6}) = [0, 90]$ deg, is visualized in Fig. 6 (b).

Control I

The Control I has been evaluated on the reference trajectory shown above by using three related configurations. First, the feed-forward (8) only has been applied. Second, the feed-forward has been augmented by the PD feedback as in (26), but without reference position transformation, i.e. $\theta_r = q_r$. Third, the complete Control I as in (26) has been applied. The control error of link positioning is shown in Fig. 7, for the 1st joint in (a) and 2nd joint in (b). One can see that already the single feed-forward control provides a relatively high positioning accuracy, up to certain numerical (integrative) errors. This argues in favor of the inverse dynamics computations (5)-(8) which are implemented with a discrete-time and discrete-state solver and are real-time compatible. The augmented feedback control, when $\theta_r = q_r$,

improves further the link position accuracy but only up to the joint torsion values. The highest accuracy is achieved in case of the full Control I as in (26). The accuracy is close to hysteresis lost motion, see Fig. 4 (b). Interesting fact is that the steady-state error at final zero-gravity position (see Fig. 7 (a) for $t > 3$ sec) is inferior for the full Control I comparing to the case when $\theta_r = q_r$. This is because the reference value transformation does not account for the actual hysteresis state which can be highly varying during a feedback regulation in vicinity to the torsion-torque origin. On the contrary, a dying-out oscillating response of the Control I with $\theta_r = q_r$ apparently drives the hysteresis to an erased (memory-free) state, thus reducing the impact of hysteresis lost motion on the link positioning error.

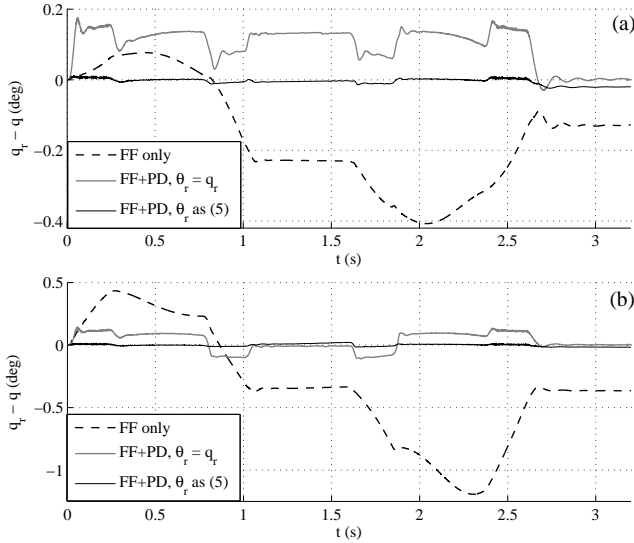


Fig. 7. Control error of the link position: 1st joint (a) and 2nd joint (b)

Control II

The Control II has been evaluated on the same reference trajectory as before, also by using three related configurations for the sake of comparison. First, only the feed-forward (FF) control \tilde{u}_r from (27) has been applied. Second, the feed-forward control has been augmented by the same PD feedback control as before (FF+PD), but with the reference $q_r = \theta$. Note that this is equivalent to a standard rigid-manipulator control (model-based feed-forward plus PD feedback) without considering the joint elasticities. Third, the full Control II as in (27) has been applied which incorporates the virtual sensor (FF+PD+VS). Recall that the VS serves for predicting the actual joint torsion as exemplary shown in Fig. 8 for the evaluated trajectory. The torsion-torque portrait, i.e. plant output, of the 1st joint is shown in Fig. 8 (a). One can see a large set of minor hysteresis loops inside of the major one. The relative torsion of the 1st joint is compared with the VS prediction in Fig. 8 (b). Both curves coincide well with each other for the transients and steady-states and zero motion as well. The VS prediction offers a slightly higher oscillating pattern which can be reduced by decreasing the L

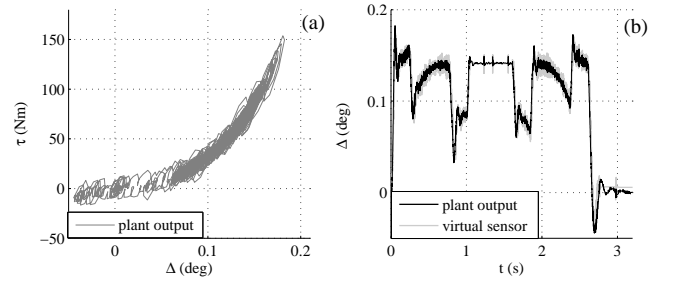


Fig. 8. Torsion behavior of the 1st joint during trajectory control; torsion-torque portrait of the plant output (a), comparison of the plant output with virtual sensor (VS) prediction (b)

gains, however at costs of the slower transients. The control error of link positioning is shown in Fig. 9, for the 1st joint in (a) and 2nd joint in (b). The FF+PD control performance is comparable with that shown in Fig. 7 for the Control I. The single FF control is, however, inferior comparing with Fig. 7, since FF in (27) constitutes a reduced feed-forwarding, i.e. without accounting for joint elasticities. The best link positioning accuracy is achieved with the FF+PD+VS control which compensates for the actual joint torsion. At the same time, the FF+PD+VS is inferior to the full Control I, compare Figs. 7 and 9. This is quite natural since the predicted torsion value, even when accurate enough, solely enters the proportional feedback control term and thus can be just as efficient as the corresponding proportional control part is. An increase of the K_p gain can further improve the steady-state performance of FF+PD+VS control, however, at costs of the higher transient overshoots. At the same time, one can notice that the Control II can better cope with hysteresis lost motion at zero gravity steady-state, compare Figs. 7 (a) and 9 (a) at time $t > 3$ s. This is quite natural since the concept of VS deals with estimating the actual hysteresis joint torsion independent of the reference trajectories and modeling of manipulator dynamics.

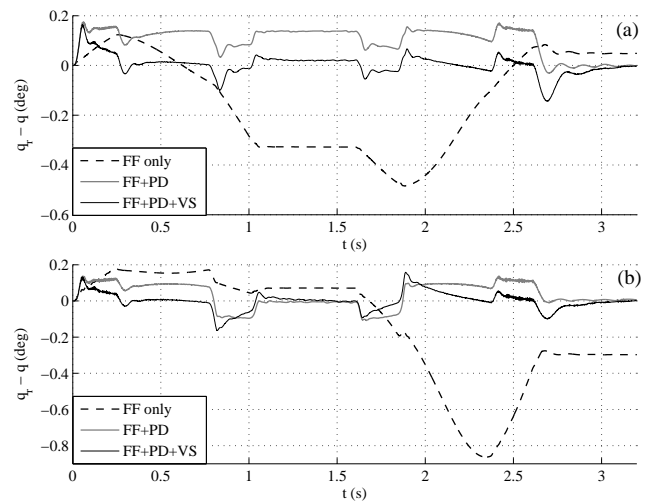


Fig. 9. Control error of the link position: 1st joint (a) and 2nd joint (b)

Discussion

Based on the description of both control methods given in Sections II and IV and control evaluation made above the following remarks can be drawn.

(i) Both methods, Control I and Control II, are the approaches to compensate nonlinear torsion that should be useful when high positioning accuracy is required. This compensation, however, in order to be effective requires an accurate modeling of the motor and gear, including friction effects. Both control methods are suitable for a multi-link robotic manipulator and account for the related multiple-input-multiple-output plant with cross-couplings. Both control methods require the nonlinear (hysteresis) torsion-torque map of each flexible joint to be identifiable and thus available as an accurate model.

(ii) The Control I provides in total the best accuracy of link positioning. At the same time, the control accuracy becomes inferior at zero gravity steady-state, where the hysteresis trajectories, close to the torsion-torque origin, give rise to residual link positioning errors. These cannot be compensated by the Control I since the latter relies on a feed-forward computation of torsion trajectories and thus does not account for actual state of the joint torsion. Another flaw of Control I is that this requires an accurate model of the multi-link robotic manipulator, including the configuration-dependent inertia and gravity terms and friction as well, see equation (8). These can change, however, during the manipulator's operation, e.g. due to an additional payload applied on the end-effector.

(iii) The Control II is slightly inferior at compensating the relative joint torsion, comparing to the Control I. Its performance is directly related to that of the underlying PD feedback control and to accuracy of predicting the actual joint torsion. The accuracy of torsion's prediction constitutes a trade-off between the fast transients of joint torque estimate and high-frequency (chattering) components at steady-states and settling from the transients. At the same time, the Control II does not require an accurate model of the multi-link robotic manipulator and accounts for the actual joint torsion state at hand. The utilized concept of virtual sensor of the joint torsion requires, however, an accurate modeling of motor drive friction and motor drive inertia. While the motor drive inertia can be assumed as constant, i.e. time-invariant, the friction can underlie large uncertainties due to e.g. thermal effects, wear, dwell time, and others. The uncertain friction behavior and its observation and compensation have been recently addressed in [25].

VI. CONCLUSIONS

In this paper, we have analyzed and compared two control approaches aimed at compensating for the nonlinear torsion in flexible joint robots. Both approaches differ in requirements posed on the available models of system dynamics and their accuracy. The first method assumes an accurate model of a rigid-link manipulator dynamics and its inverse. Based thereupon the reference trajectory is transformed from the link space into that of the motor drives, which are under

a closed-loop control. The PD feedback control is combined with the full-order reference torque feed-forwarding. The second method relies on an accurate model of the motor drives and allows for observing the reactive joint torque based on the generalized momenta. The observed reactive joint torque allows for computing the relative joint torsion. Thus, the motor drive feedback control operates in the 'virtual' joint link space by accounting for torsion. Both approaches make use of the same torsion-torque hysteresis map and its inverse. It turns out that depending on the model availability and control specification each of the methods can offer several assets and drawbacks. The simulation example of a two-link planar manipulator under gravity showed the applicability of both control methods.

REFERENCES

- [1] M. Readman, *Flexible joint robots*. CRC press, 1994.
- [2] M. W. Spong, S. Hutchinson, and M. Vidyasagar, *Robot modeling and control*. Wiley, 2006.
- [3] B. Siciliano, L. Sciavicco, L. Villani, and G. Oriolo, *Robotics: modeling, planning and control*. Springer, 2009.
- [4] P. Tomei, "A simple PD controller for robots with elastic joints," *IEEE Transactions on Automatic Control*, vol. 36, no. 10, pp. 1208–1213, 1991.
- [5] M. W. Spong, "Modeling and control of elastic joint robots," *Journal of Dynamic Systems, Measurement, and Control*, vol. 109, no. 4, pp. 310–319, 1987.
- [6] A. De Luca, B. Siciliano, and L. Zollo, "PD control with on-line gravity compensation for robots with elastic joints: Theory and experiments," *Automatica*, vol. 41, no. 10, pp. 1809–1819, 2005.
- [7] M. Ruderman, T. Bertram, and M. Iwasaki, "Modeling, observation, and control of hysteresis torsion in elastic robot joints," *Mechatronics*, vol. 24, no. 5, pp. 407–415, 2014.
- [8] M. Ruderman and M. Iwasaki, "On identification and sensorless control of nonlinear torsion in elastic robotic joints," in *40th IEEE Annual Conference Industrial Electronics Society (IECON-2014)*, Dallas, 2014, pp. 2828–2833.
- [9] T. D. Tuttle and W. P. Seering, "A nonlinear model of a harmonic drive gear transmission," *IEEE Transactions on Robotics and Automation*, vol. 12, no. 3, pp. 368–374, 1996.
- [10] H. D. Taghirad and P. R. Bélanger, "Modeling and parameter identification of harmonic drive systems," *Journal of Dynamic Systems, Measurement, and Control*, vol. 120, no. 4, pp. 439–444, 1998.
- [11] F. Ghorbel, P. Gandhi, and F. Alpetter, "On the kinematic error in harmonic drive gears," *Journal of Mechanical Design*, vol. 123, no. 1, pp. 90–97, 2001.
- [12] R. Dhaouadi, F. H. Ghorbel, and P. S. Gandhi, "A new dynamic model of hysteresis in harmonic drives," *IEEE Transactions on Industrial Electronics*, vol. 50, no. 6, pp. 1165–1171, 2003.
- [13] N. Kircanski, A. Goldenberg, and S. Jia, "An experimental study of nonlinear stiffness, hysteresis, and friction effects in robot joints with harmonic drives and torque sensors," in *Experimental Robotics III*. Springer, 1994, vol. 200, pp. 326–340.
- [14] W. Seyffarth, A. J. Maghzal, and J. Angeles, "Nonlinear modeling and parameter identification of harmonic drive robotic transmissions," in *Proc. IEEE International Conference on Robotics and Automation (ICRA'95)*, vol. 3, 1995, pp. 3027–3032.
- [15] A. Astolfi, D. Karagiannis, and R. Ortega, *Nonlinear and adaptive control with applications*. Springer, 2007.
- [16] M. Ruderman and M. Iwasaki, "Impact of hysteresis lost motion on the sensorless torsion control of elastic robotic joints," in *IEEE International Conference on Mechatronics (ICM2015)*, Nagoya, 2015, pp. 650–655.
- [17] M. Ruderman and M. Iwasaki, "Sensorless torsion control of elastic joint robots with hysteresis and friction," *IEEE Transactions on Industrial Electronics*, vol. PP, no. 99, pp. 1–1, 2015.
- [18] A. De Luca, "Feedforward/feedback laws for the control of flexible robots," in *IEEE International Conference on Robotics and Automation (ICRA'00)*, 2000, pp. 233–240.

- [19] B. Armstrong, P. Dupont, and C. C. De Wit, "A survey of modeling, analysis tools and compensation methods for the control of machines with friction," *Automatica*, vol. 30, pp. 1083–1138, 1994.
- [20] F. Al-Bender and J. Swevers, "Characterization of friction force dynamics," *IEEE Control Systems Magazine*, vol. 28, no. 6, pp. 64–81, 2008.
- [21] C. De Persis and A. Isidori, "A geometric approach to nonlinear fault detection and isolation," *IEEE Transactions on Automatic Control*, vol. 46, no. 6, pp. 853–865, 2001.
- [22] A. De Luca and R. Mattone, "Actuator failure detection and isolation using generalized momenta," in *Proc. IEEE International Conference on Robotics and Automation (ICRA'03)*, 2003, pp. 634–639.
- [23] M. Ruderman, *Modeling of Elastic Robot Joints with Nonlinear Damping and Hysteresis*. Rijeka, Croatia: InTech, Open Access Publisher, 2012, ch. 15, pp. 293–312.
- [24] B. J. Lazan, *Damping of materials and members in structural mechanics*. Pergamon press Oxford, 1968, vol. 214.
- [25] M. Ruderman and M. Iwasaki, "Observer of nonlinear friction dynamics for motion control," *IEEE Transactions on Industrial Electronics*, vol. 62, no. 9, pp. 5941–5949, 2015.